Innovative antennas for next generation of communication systems in Vietnam

Innovative Antennas for next generation of communication systems in Vietnam

Andrea Massaccesi[1], Michele Beccaria[1], Ho Man Linh[2], Nguyen Huu Trung[2], Nguyen Khac Kiem[2], Paola Pirinoli[1]

[1]Dept. of Electronics and Telecomm. – Politecnico di Torino, Torino, Italy, [2]Dept. of Aerospace Electronics - Hanoi University of Science and Technology, Hanoi, Vietnam

Abstract

Vietnam is one of the first countries in the world to successfully test the 5th Generation Mobile Network or simply 5G service. At the test, mobile internet speed has reached 1.7 Gbps, much faster than 4G and equivalent to the speed of commercial cables. 5G is recognized as the foundation for implementing the Industrial Revolution 4.0 to deploy digital economy, smart cities, smart environment, electronic citizens and goverment in countries like Vietnam. To satisfy all these requirements, a notable effort in the research and exploration of novel and revolutionary technologies was done and it is still on going. In particular, the need of high data rates can be satisfied increasing the available frequency bands and the spectral efficiency. At its turn, it can be obtained with the use of massive Multiple-Input Multiple-Output (MIMO) architectures. MIMO antennas are characterized by a number of radiating elements larger than the served user terminals, so that it is possible to enhance the throughput capacity. The design of an efficient MIMO system involves two main aspects, both considered here: the design of the actual antenna and of the beamforming algorithm. Different possible solutions are considered, and their performance are compared.

1 Introduction

The new standard of communication systems will be the 5G, that is expected to achieve higher performance than the previous protocols, i.e. 3 or 4G. The high demand of customers to exchange a huge quantity of data, the need of high speed of streaming and buffering (for HD movies, heavy online videogames etc.) should be served by a sophisticated technology which would be able to perform an increased rate of 1000 times with a data rate of 1 Gb/s, a latency lower than 1 ms, reduced energy consumption and costs. Moreover, 5G will be a system also suita-

ble to provide a lifeline communication in case of a natural disaster connecting at the same time a lot of users without the interruption of the services [1]-[2]. Another important aspect of the user experience is the Cloud service that is expected to exponentially grow (above 90%) [4] in the next years, because of the interest in users to manage big data rates everywhere with their "own device" without an expensive hardware.

In view of all these requirements, the use of a technology able to increase wireless channel capacity without additional power and spectrum is almost mandatory. One of the most promising solution is represented by the use of a MIMO antenna system, whose higher efficiency is due to the use of multipath to increase the channel throughput.

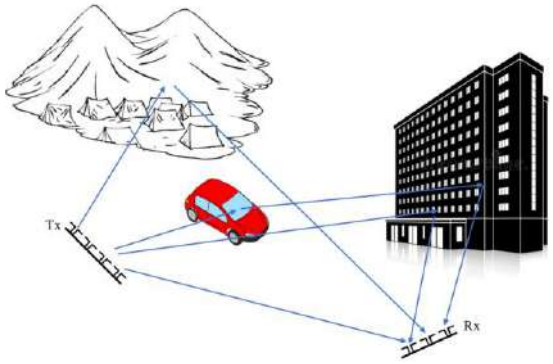

Figure 11 - Sketch of an outdoor environment, where several transmitting and receiving devices are present. The wireless connection is carried on taking advantage from the multiple reflections as in a MIMO system.

To understand how a MIMO system works, let consider the case of an array, made up of *N* elements, that send data to *M* separate users. If its beamforming is designed in such a way that the antenna radiates several patterns (i.e. it shows a multibeam behavior), each one transmitting data just to a single user and if each radiation pattern encodes a different data stream, the entire system can transmit simultaneously to all the users with a spectral occupancy equal to that of a single transmission. Something of similar happens in MIMO antennas: if between the Tx and the Rx there are several possible paths as sketched in Fig. 1, each of them can transmit a different data stream, increasing the channel throughput. This is called spatial multiplexing (SM). Within the transmitter, each data stream may be separately applied to the *N* transmit antennas and propagated over multipath channel to a receiver. Error correction coding may be applied to each of the data stream separately or in a combined space-time coding method. MIMO technology also offers diversity gain and array gain. MIMO provides more robustness against signal in-

terference by beamforming and/or nulling techniques. For a fixed overall transmitted power, the capacity offered by a MIMO configuration may scale with the increased signal-to-noise ratio (SNR). Array gain increases the received carrier-to-noise-ratio (CNR) with coherent signal combination at the receive side. Channel state information (CSI) is required at both transmitter and receiver with the help of pilot signals [1].

Massive MIMO systems employ a large number of transmit and receive antennas (usually greater than 100 elements), have been of great interest in recent years because of their potential to dramatically improve spectral efficiency of future wireless systems and increase the transmission data rate through spatial multiplexing to deliver multiple streams of data within the same resource block (time and frequency). Massive MIMO systems exploit multipath propagation to improve the system reliability in terms of bit error rate (BER) performance, without the expense of additional bandwidth. Moreover, massive MIMO, can increase the power efficiency by scaling down the transmit power of each terminal inversely proportional to the number of elements of antenna array at base stations. It can steer multiple beams to a number of user ends to enhance SNR ratio [2].

The design of a MIMO system involves both that of the actual antenna as well as that of the beamforming. An appropriate beamforming algorithm is needed to transmit the signal to desired users or receive the signal in a desired direction in order to overcome frequent LOS blockages and rich scattering multipath propagation in the mm-wave channel. The very small wavelengths of mm-wave frequencies allow to incorporate a large number of antenna elements in a compact form factor to generate sharp beams corresponding to large array gains. For example, when using squared flat antenna array with half-wavelength uniform spacing between elements of the array in 20 GHz frequency band, the dimension of the 256-element array is only 12 cm square.

The radiation features of the MIMO system can be obtained adopting a multibeam antenna, able to cover different angular region and to radiate inside each of them a sufficiently high gain. They can be realized exploiting different technologies [6], [7] that could be grouped in two different classes, that of the antenna using active components and the other ones that are passive structures. In Active Multibeam Antennas (AMBAs) the direction of maximum radiation is controlled electronically: the resulting performances are generally excellent, but the use of beamforming networks and active components make the antenna difficult to design and expensive to manufacture. In Section 2, considerations on multibeam phased arrays and in particular on the beam forming are discussed.

The second alternative is represented by Passive Multibeam Antennas (PMBAs) whose main advantages are that of a lower cost and easier manufacturing. Among the possible types of PMBA there is that by adopting a passive aperture antenna illuminated by the field radiated by a feed-array: even if the most traditional configurations use a shaped reflector or a dual reflector system to improve the antenna performances, other possible solutions consist in substituting the metallic, bulky reflector with a planar Reflectarray (RA) [8], or in using a device

working in transmission, i.e. a lens or a planar Transmitarray (TA) [9], [10], presenting the advantage that it could be designed with a centered feeding system, since it does not suffer for problems related to the blockage.

In Section 3 some results on the possibility to use a TA for the realization of an efficient PMBA will be presented; the focus is on the requirements that a transmitarray has to satisfy to overcome its intrinsic limitations in multibeam applications. Some considerations on the effect of the unit cell will be firstly presented, then possible techniques for the efficient design of the TA will be discussed.

2 Multi-beam phased arrays

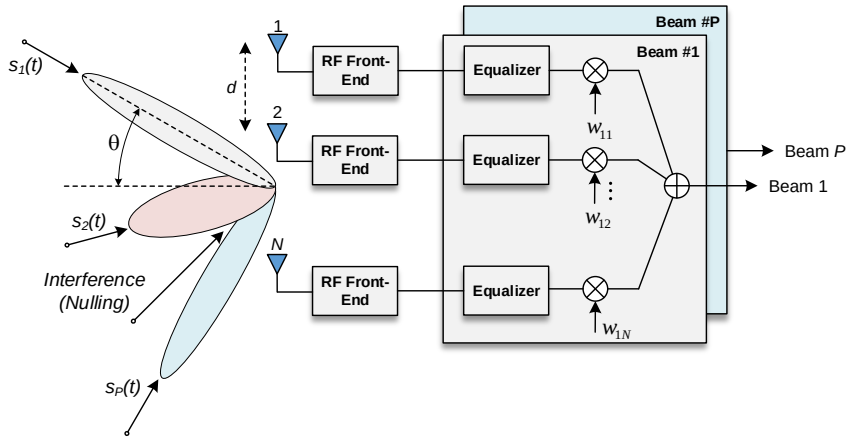

Figure 12 - Multi-beam phased array architecture.

Multiple beamforming is a technique that uses antenna arrays to produce a number of simultaneously available adjustable radiation patterns, which can point to the desired coverage areas and minimize the impact of unwanted noise and interference, thereby improving the quality of the desired signal. Basically, beamforming is an optimal spatial filter [3]. Antenna arrays using a beamforming technique can eliminate interferences having a direction of arrival different from that of the desired signal. Multi-polarized arrays can also eliminate undesired signals having a polarization different from that of the desired signal, even if the signals have the same direction of arrival.

Beamformers use an array of antenna elements that are individually phased in such a way as to form beams (or nulls) in a desired direction. Let consider a multiple beamforming system. The inter-element distance is *d*. The system has *N* antenna elements for multiple beamforming. The system model is illustrated in Fig.

2. If $s_i(t)$ is the signal associated to the i^{th} beam and the pointing angle associated with $s_i(t)$ is θ_i, the vector of array transmitting from N elements at time instant t is expressed as:

$$\mathbf{x}_i(t) = \boldsymbol{a}_i(\theta_i, \omega_i)s_i(t) \tag{1}$$

where $\mathbf{x}_i(t) = [x_{i1}\ x_{i2}\ \dots\ x_{iN}]^H$ collects the signal samples received at the antennas and $\boldsymbol{a}_i(\theta_i, \omega_i)$ is the steering vector according to $s_i(t)$:

$$\boldsymbol{a}_i(\theta_i, \omega_i) = \left[1\ \ e^{j\omega_i dsin(\theta_i)/c} e^{j\omega_i 2dsin(\theta_i)/c} \dots\ \ e^{j\omega_i (N-1)dsin(\theta_i)/c}\right]^H \tag{2}$$

In the above equation, ω_i indicates the carrier frequency and c the speed of light. The steering vector depends on the direction of departure and the frequency. For simplicity, we denote $\boldsymbol{a}_i(\theta_i, \omega_i)$ with $\boldsymbol{a}_i$. The single beamforming model is therefore expressed as $\mathbf{x}_i(t) = \boldsymbol{a}_i s_i(t)$ and he multiple beamforming model becomes:

$$\mathbf{x} = \mathbf{A}\boldsymbol{s} \tag{3}$$

where $= [\boldsymbol{a}_1(\theta_1, \omega_1), \boldsymbol{a}_2(\theta_2, \omega_2), \dots \boldsymbol{a}_P(\theta_P, \omega_P)]$, $\mathbf{x} = [\mathbf{x}_1, \mathbf{x}_2, \dots \mathbf{x}_P]^T$ and $\boldsymbol{s} = [s_1, s_2, \dots s_P]^T$ for the P beams.

There are two general beamforming systems: narrow band beamforming and broad band beamforming. In narrow band beamforming model, the output signal $y_i(t)$ of the beamformer i (i=1,…, P) at the time instant t is obtained by linear combination of the signals of N elements as:

$$y_i(t) = \sum_{j=1}^{N} w_{ij}^* x_{ij}(t) \tag{4}$$

For broadband model, the output signal is expressed as:

$$y_i(t) = \sum_{j=1}^{N} \sum_{p=0}^{K-1} w_{ij,p}^* x_{ij}(t-p) \tag{5}$$

where $K-1$ is the number of delay stages of the equalizer at each channel of the i^{th} element of the array. The transmitted signal is expressed as:

$$y_i(t) = \boldsymbol{w}_i^H \mathbf{x}_i(t) \tag{6}$$

where $\mathbf{x}_i$ is the signal vector. The vector $\boldsymbol{w}_i^H$ of length N represents the weights as:

$$\boldsymbol{w}_i^H = [w_{i1}^*, w_{i2}^*, \dots, w_{iN}^*] = [\boldsymbol{w}_i^H]^* \tag{7}$$

and so the response of the i^{th} beamformer is expressed as:

$$r_i(\theta_i, \omega_i) = \boldsymbol{w}_i^H \mathbf{a}_i \tag{8}$$

The beam pattern is defined as the squared magnitude of $r_i(\theta_i, \omega_i)$. Note that each of the weight coefficient in the weight vector impacts on the response of the beamformer in terms of time and space.

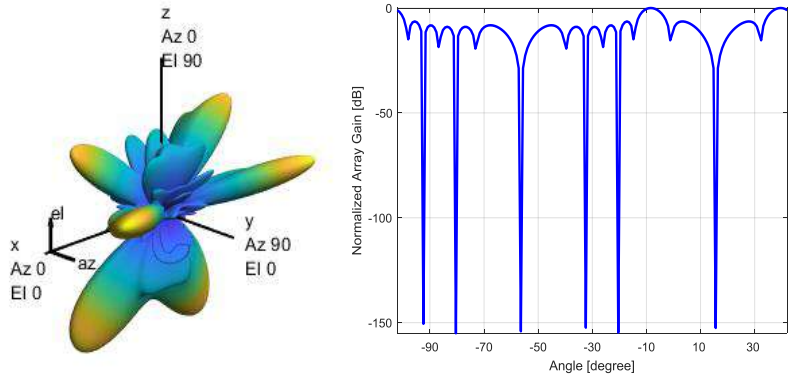

Figure 13 - 3D beampattern (left) and array gain with nulling (right) of a multi-beam phased array.

2.1 Millimeter-wave Beamforming

The obvious advantage of using millimeter-wave (mm-wave) bandwidth is the availability of under-utilized contiguous spectrum. These bands allow wide bandwidth up to 400 MHz and support up to 1.2 GHz of instantaneous bandwidth with carrier aggregation [4].

Depending on the beamforming architecture, the beamforming weights required to form the beam pattern could be applied in the digital or analog domain. For MIMO systems, all-digital beamforming is usually implemented in the form of digital precoding that multiplies a particular coefficient to the modulated baseband signal per RF chain. On the other hand, for analog beamforming, complex coefficients are applied to control the directive beam through phase shifters with variable gain amplifiers if needed. In general, all-digital beamforming offers a higher degree of freedom and better performance at the expense of increased complexity and cost. Analog beamforming, on contrary, is a simple and effective method of generating high beamforming gains from a large number of antennas but less flexible than the other method.

The all-digital beamforming architecture for sub-6 GHz MIMO platform and the advanced signal processing algorithms for spatial multiplexing was first extended to mm-wave beamforming. However, the baseband and MIMO precoding structure in the sub-6 GHz system cannot be applied directly into the mm-wave systems [5] because the baseband precoding requires a complete dedicated RF

chain with very high speed ADC/DAC for each antenna element at the transmitter or the receiver, which is expensive and highly complex.

To obtain the advantages of massive MIMO and also provide high array gain to compensate for the large path loss at mm-wave bands, the hybrid beamforming structure has been proposed as an enabling technology for 5th Generation Mobile Network [6]. This is trade-off solution between flexibility and performance and bring the mm-wave beamforming to practical implementation. The hybrid beamforming structure for the mm-wave transmitter is illustrated in Fig. 4.

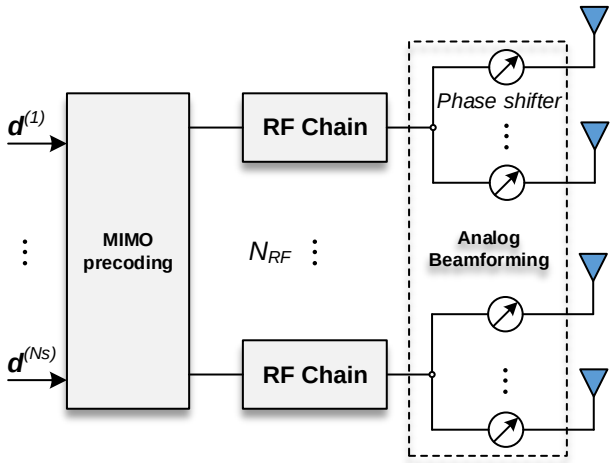

Figure 14 - Hybrid beamforming structure for the mm-wave transmitter.

As it can see in the block diagram, N_s data streams are fetched to the MIMO precoding, normally spatial multiplexing and then the output is through the N_{RF} RF chains. The beamformer function splits the RF signal into P beams to feed each active element of the phased array. It provides high-resolution phase and amplitude weighting, which is needed to synthesize beamforming patterns and adaptively null potential interferences. The RF chain blocks for OFDM modulation often include ITTF, P/S (parallel to serial), CP (cyclic prefix insert) and DAC to form output signal. The mixer converts the baseband signal up to carrier frequency. The final block of RF chain which is close to the antenna is the front-end, which contains a high-power and high-efficiency transmit PA, a transmit/receive switch, and low-noise amplifier (LNA) [7].

3 Multi-beam transmitarray

A transmitarray antenna is a structure composed by a planar transmitting surface and a feed source, that in fixed beam applications consists in most of the cases in a horn (see e.g. [11] and references therein). The TA surface is designed in such a way that, for a given position and type of the feed, it transforms the incoming spherical wave front in a planar phase front. To overcome the lack of curvature, the TA surface is discretized with a proper number of Unit-Cells (UCs), having size lower or equal to half of the wavelength ($\lambda_0/2$) at the design frequency f_0: each of them can control the phase and the amplitude of the transmission coefficient S_{21}, that are locally changed varying one or more geometrical parameter of the unit cell itself, in such a way to adjust the phase of the incident field, that at its turn depends on the relative position of the feed and the TA. The resulting antenna is generally characterized by a high gain in the selected direction of maximum radiation.

In the case of a multibeam system, things are a little more complex. If it is a passive configuration, the generation of the different beams can be obtained substituting the single feed with a focal feed array: as can be seen from the drawing in Fig. 5, it generates simultaneously more beams, that impinge on the TA surface with a different incident angle and therefore the transmitarray radiates a beam in a different direction for each of them.

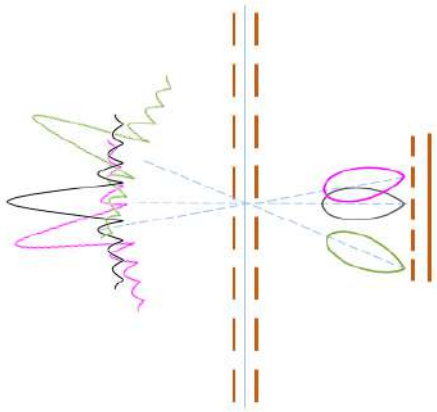

Figure 15 - Working principle of a multibeam TA: each element in the feed array radiates a beam in a different direction, that impinges on the transmitarray with a different angle of incidence that generate a beam in the consequent direction

Ideally, the TA might be able to radiate in almost the same way in all the directions, i.e. the radiation patterns generated by beams arriving from the different incident direction must present almost the same gain, Half Power Beam Width (HPBW) and Side Lobe levels (SLL). Unfortunately, this is difficult to obtain, mainly for the two following reasons:

- the behavior of the unit cell depends on the direction of arrival of the incident wave;
- the procedure for the TA design described above guarantees a good performance for a fixed position of the feed, but not when it is moved.

In view of these considerations, the following analysis has been carried on. First, two different types of unit cell have been considered, and their effect of the entire antenna performance has been studied and compared; then the effect of the position of the feed with respect to the TA has been analyzed and finally the possibility to use a different design procedure has been exploited. Some of the obtained results are summarized in the following. They have been got with the full-wave numerical analysis of a reduced size transmitarray ($10\lambda_0 \times 10\lambda_0$), carried on with CST Microwave Studio. Since the multibeam transmitarray is thought as the possible radiating system in a MIMO configuration for 5G, the selected operating frequency is in one of the bands that will be used for this service, and it is equal to $f_0 = 5.8$ GHz [12]-[13].

3.1 Transmitarray unit-cell

In order to investigate the relation between the behavior of the unit cell as a function of the direction of arrival of the incident field and the capabilities of beam steering of the TA, two different UCs have been analyzed.

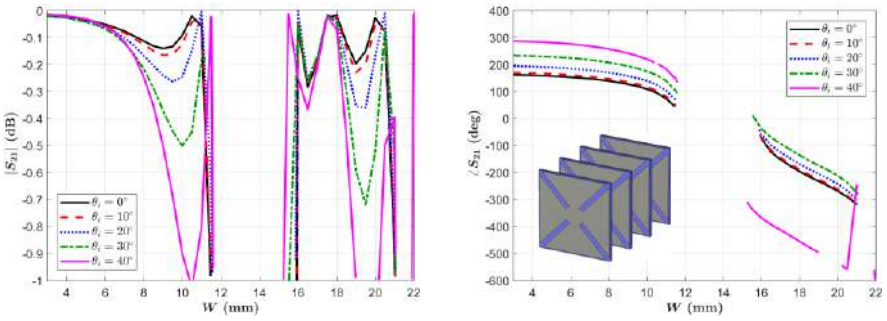

Figure 16 - Variation of the amplitude (left) and phase (right) of S_{21} versus W for several angle of incidence. Inset: unit cell.

The first one is the classical multilayer printed structure shown in Fig. 6. Each layer is characterized by a relative dielectric constant $\mathcal{E}_r = 2.574$, a thickness h= 0.5 mm, negligible losses; the spacing between two following layers are chosen in such a way that the total distance between two printed elements is almost $\lambda_0/4$ at the design frequency f_0 in order to maximize the transmission coefficient. The unit-cell size is $\lambda_0/2$, with the aim to avoid grating lobes. The variation of the transmission coefficient is controlled through the side W of the printed elements, that have the shape of a Malta cross.

In Fig. 6, the variation of the phase and amplitude of S_{21} with W, and for different angles of incidence, is plotted. They have been computed using the Floquet excitations in CST MWS®. Because of the presence of higher order mode resonance, it happens that for some values of W the phase of the transmission coefficient presents discontinuities and its magnitude strongly decrease; this phenomenon is already noticeable in the case of normal incidence ($\theta = 0°$), but it is more evident for higher values of the incident angles. To avoid the problems that such a behavior could have it has been decided to "cut" the curves in correspondence of these resonances, and the corresponding values of W are discarded. While in case of normal incidence the unit cell guarantees a phase variation of 370° and losses not greater than -1 dB, for other values of θ, both the phase and the amplitude of S_{11} changed drastically, and therefore a different behavior of a TA using this kind of element for different position of the feed is predicted.

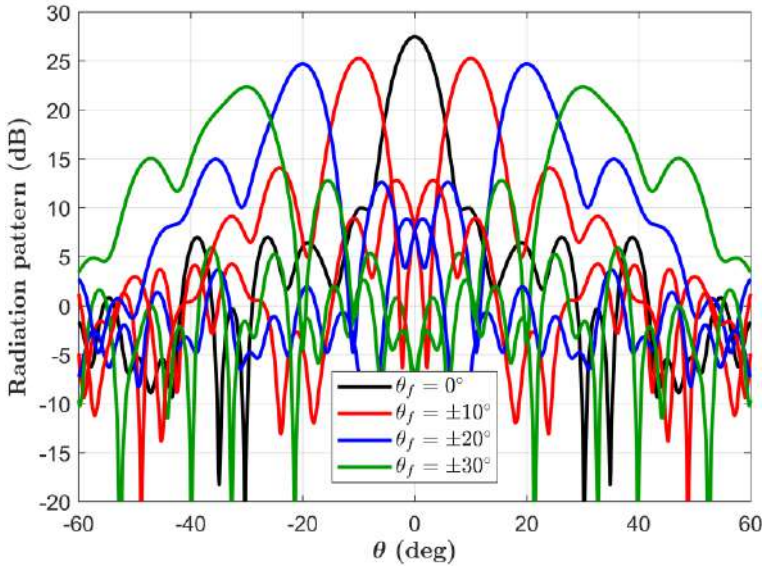

Figure 17 - Radiation patterns in the E-plane relative to the Malta cross TA, illuminated by a horn that rotates along an arc centered in the center of the transmitarray aperture.

This hypothesis is confirmed by the radiation patterns shown in Fig. 7. They refer to a $10\lambda_0 \times 10\lambda_0$ transmitarray, designed using the multi-layer Malta cross as unit cell. The value of W for each of them has been fixed assuming the feed centered with respect to the TA and located at $9\lambda_0$ from its surface. To obtain the beam in the different directions, the feed has been rotated along a circular arc, as can be seen in Fig. 8, on the left.

As it can be seen, there is a noticeable degradation of the radiation patterns, starting from the broadside direction to the maximum scanning angle. The gain loss is of almost 5 dB, and the SLL increases drastically.

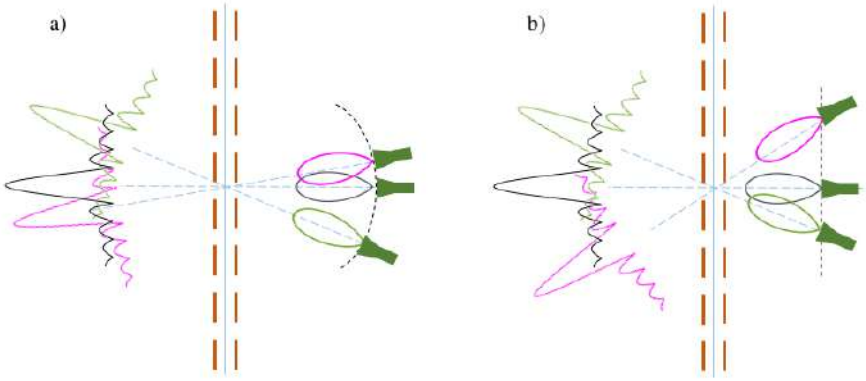

Figure 18 - The two analyzed TA configurations: (a) the feed rotates along a circular arc; (b) the feed moves parallel to the TA surface, as in a feed array.

The second unit cell that is considered has been recently introduced in [14] and experimentally validated in [15]-[16]. It is composed by three dielectric layers of the same material (see inset in Fig. 9) and has a periodicity *W* in both x and y directions. The central layer is characterized by a square hole of height H_{sqh} and size *d*, that is used to control the phase of the transmission coefficient. The two external, identical layers present a hole that has a truncated pyramid shape with height H_{tap} and they act as a broadband matching circuit, allowing to improve the performance of the dielectric unit-cell in terms of bandwidth and reduce the dependence from the angle of incidence. Moreover, the dielectric UC has the advantage that it can be realized using Additive Manufacturing (AM) techniques, as demonstrated in [12]-[13].

In view of its advantages, the selected material for the realization of the TA has been the commercial 3D-printable Preperm® L700HF, which is characterized by $\mathcal{E}_r = 7$ and $\tan\delta = 0.001$. This material can be provided as filaments and printed through Fused Deposition Modeling (FDM) processes. The high value of the dielectric constant is favorable for reducing the thickness of the cell and therefore the dielectric losses. The periodicity of the cell is W =13 mm $\simeq \lambda_0/4$, while the heights are $H_{sqh} = H_{tap}$ = 24 mm $\simeq 0.46\lambda_0$, corresponding to a total cell thickness $T = H_{sqh} + 2H_{tap}$ = 72 mm $\simeq 1.38\lambda_0$. The hole size *d* is varied from 1 to 12 mm to obtain a full phase range of 360°.

Also in this case, the transmission coefficient of the unit-cell has been computed using Floquet excitations in CST MWS®. Fig. 9 shows the variation of the transmission coefficient magnitude (left) and phase (right) with *d,* evaluated for

different incidence angles (θ_i). The magnitude slightly degrades when the angle of incidence increases, with a reduction not greater than 0.7 dB for θ_i = 40°, while from the curves of the phase variation it emerges that all of them provide a full phase range of 360° and remains linear and quite similar for the different θ_i. They maintain almost the same slope until half of the range of d, then, the slope slight changes, arriving to have the maximum difference at the upper limit of the range. These results suggest that the designed unit cell is not particularly sensitive to the angle of incidence, making it a potential good candidate to be used in the design of transmitarrays with multibeam capabilities.

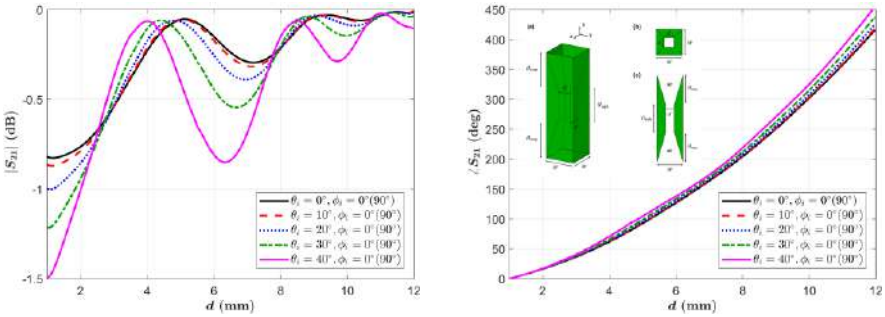

Figure 19 - Variation of the amplitude (left) and phase (right) of S_{21} versus W for several angle of incidence. Inset: unit cell.

As for the other unit cell, a reduced size TA has been designed, with geometrical parameters (size, focal distance, feed movement) comparable with those of the TA using Malta cross UC. In Fig. 10, the radiation patterns in the E-plane (where the rotation of the feed occurs), for the scanning in the overall angular region are shown. From their comparison with the pattern in Fig. 7, it clearly emerges that the low sensitivity of the unit cell from the direction of arrival of the incident field has a strong impact on the antenna performance. In fact, here the radiation patterns stay almost the same till to θ_f = ±30°, showing a small reduction of the gain and a reduced increase of the SLL.

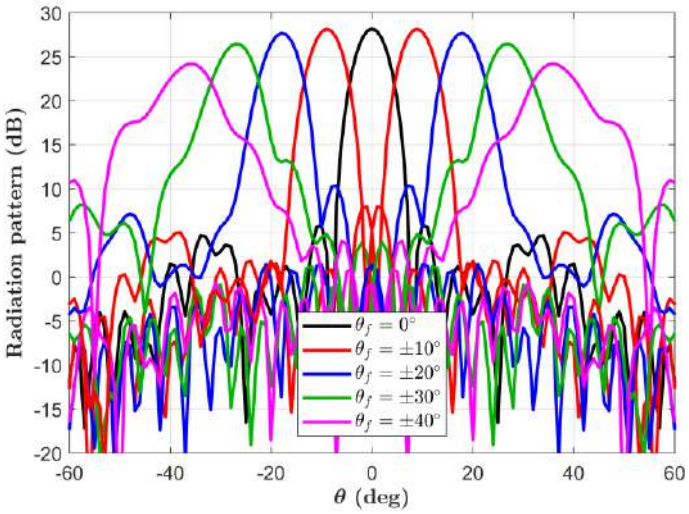

Figure 20 - Radiation patterns in the E-plane relative to the dielectric TA, illuminated by a horn that rotates along an arc centered in the center of the transmitarray aperture (configuration in Fig. 8a).

3.2 Transmitarray feed movement

The results presented in the previous sub-section have been obtained assuming that the feed rotates along a circular arc, as drawn in Fig. 8a. If this hypothesis is sufficiently accurate for what was of interest there, it is necessary to point out that the elements of a feed array illuminate the TA surface in a different way. To mimic more accurately this situation, it is possible to consider a configuration as in Fig. 8b, where the feed moves linearly and always stay parallel to the TA. This means that the distance between the feed and the transmitarray is no longer constant, and that it is lower for smaller angles of incidence.

Using this illumination mechanism, a new TA with the same size of the conventional TA has been designed and numerically analyzed. The maximum distance of the feed from the TA is $9\lambda_0$ and it is achieved for the scanning angles $\theta_f = \pm 30°$, while the minimum distance of $7.8\lambda_0$ occurs for $\theta_f = 0°$. Fig. 11 shows a comparison between the radiation patterns in E-plane relative to the conventional TA described in the previous section and this new configuration. The radiation patterns corresponding to the same value of θ_f are very similar, with comparable HPBW and SLL.

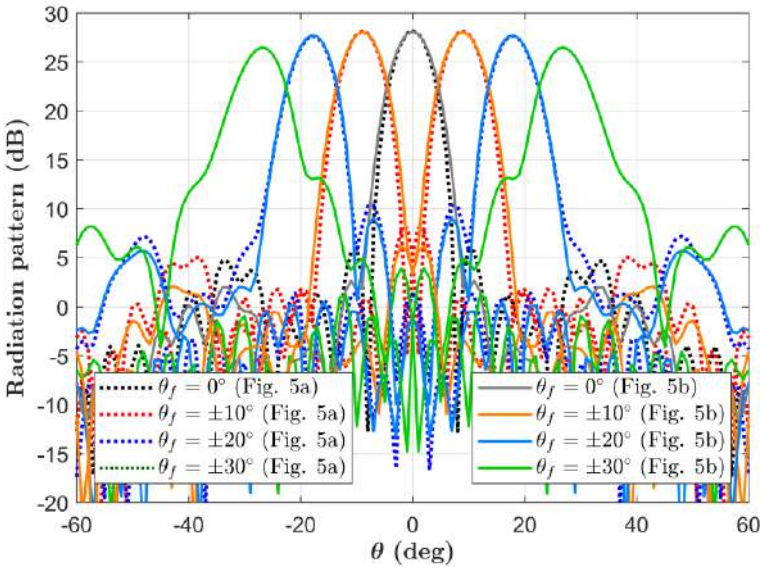

Figure 21 - Radiation patterns in the E-plane relative to the dielectric TA, illuminated by a horn that translates parallel to the TA as in Fig. 8b (dotted line) and compared with the case in which the horn rotates along a circular arc as in Fig. 5a (solid line).

3.3 Enhanced techniques for the design of a multibeam TA

The above results prove the feasibility of a multibeam TA, provided that a suitable unit-cell is adopted, but also highlight that if the TA is designed assuming a fixed position of the feed its performances are good over a limited angular range. To overcome this limitation a different design procedure must be adopted, that takes into account the different directions of arrival of the field radiated by the feed.

A possible solution is that of using a global optimizer; in Chapter **X** results on the application of two different algorithms to the design of a scanning beam reflectarray are presented: similarly to what is described there, the same approach can be also used for the transmitarray, and it is expected that in this way it would be possible to enlarge the beam steering capabilities of the antenna at least to an angular range of 80°.

Another solution, investigated in the following, consists in designing the TA as it was a bifocal lens. The main steps of this procedure are the following:

- the feed is assumed to be in an offset position, with the main beam that forms a certain angle $\theta_1$with the z-axis, and the required phase distribution φ_1 is computed;
- then, the feed is rotated forming an angle θ_2 while keeping the same distance of the feed from the center, and another phase distribution φ_2 is computed;
- Since the unit cells can compensate only one phase requirement, they cannot to compensate both φ_1 and φ_2, and therefore each element can provide a phase φ_{BFM} that is the mean value between φ_1 and φ_2.

In Fig. 12, the phase distributions φ_1, φ_2 and φ_{BFM} relative to a TA adopting as unit cell the dielectric one, with size and focal ratio equal to those of the configurations already analyzed is shown. The radiation patterns for several values of the angle of incidence, varying between −40◦ and +40◦ have been computed through a full-wave simulation of the entire antenna, and in Fig. 13 those in the E plane are plotted.

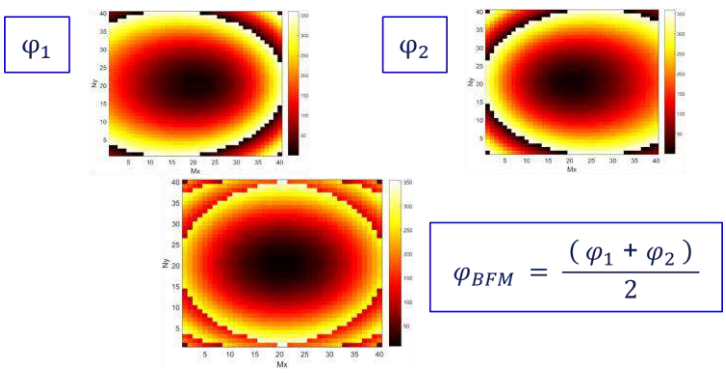

Figure 22 - Example of phase distributions used by the bifocal approach to design the TA.

The solid curves represent the results obtained with the traditional design, the dotted are referring to the bifocal method. These results prove that the bifocal TA has greater scanning capabilities, for angles of incidence not larger than 30° the gain patterns have almost the constant values and low side lobes. When the direction of maximum radiation approaches 40°, the gain decreases a little, but the main beam keeps its shape, and the side lobes stay low.

The variation of the gain as a function of the scanning angle is finally reported in Fig. 14, with that of the conventional TA illuminated with the feed moving along an arc (solid line) or linearly (dashed line). These latter are almost equal and

have a higher gain in the broadside direction, but it decreases rapidly for the other directions of maximum radiation. On the contrary, the gain for the bifocal TA varies of almost 1 dB on the entire angular range.

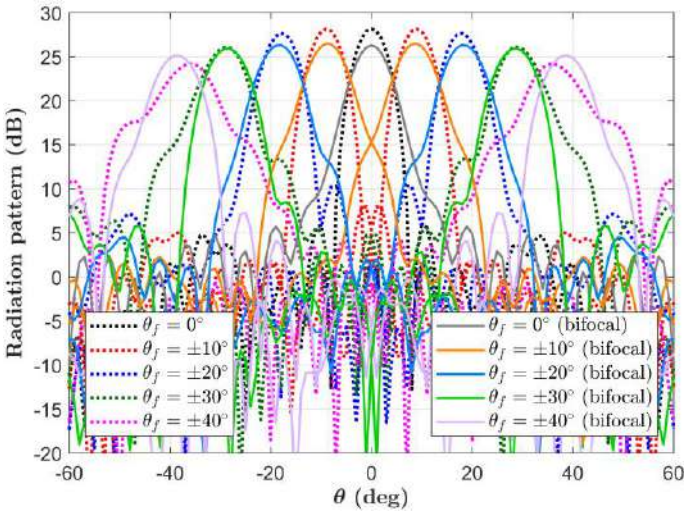

Figure 23 - Radiation patterns in the E-plane relative to the dielectric TA, designed with the bifocal method, compared with those obtained with the configuration in Fig. 8a.

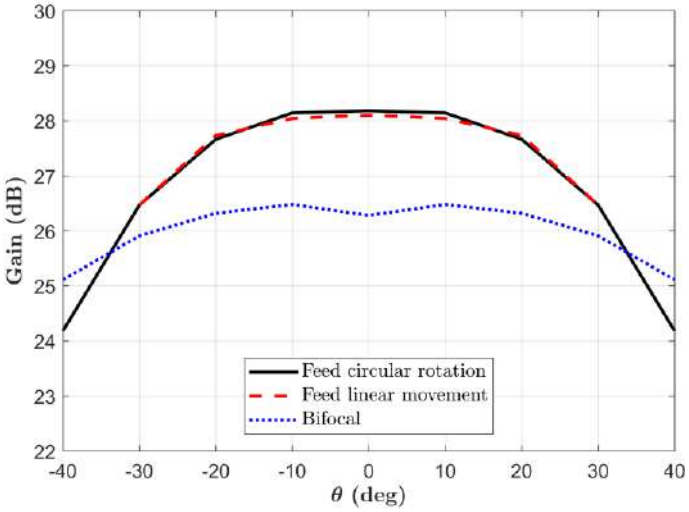

Figure 24 - Variation of the gain versus scanning angles. Comparison among the conventional TA, illuminated with a feed that moves along a circular arc (solid line) or linearly (dashed line), and the bifocal TA (dotted line).

References

1. J. G. Andrews et al., "What will 5G be?," IEEE J. Sel. Areas Commun., vol. 32, no. 6, pp. 1065–1082, Jun. 2014.
2. E. Dahlman, et al., "5G wireless access: Requirements and realization," IEEE Commun. Mag., vol. 52, no. 12, pp. 42–47, Dec. 2014.
3. T. L. Marzetta, "Noncooperative cellular wireless with unlimited numbers of base station antennas," IEEE Trans. Wireless Commun., vol. 9, no. 11, pp. 3590–3600, Nov. 2010.
4. Rath Vannithamby, Shilpa Talwar, "5G", Wiley Telecom, 2017.
5. E. G. Larsson, O. Edfors, F. Tufvesson, and T. L. Marzetta, "Massive MIMO for next generation wireless systems," IEEE Commun. Mag., vol. 52, no. 2, pp. 186–195, Feb. 2014.
6. Wei Hong, *et al*., "Multibeam Antenna Technologies for 5G Wireless Communications," IEEE Trans. Antennas Propag., vol. 65, no. 12, pp. 6231–6249, Dec. 2017.
7. B. Jokanovic, V. Milosevic, M. Radovanovic and N. Boskovic, "Advanced antennas for next generation wireless access," *2017 13th Int. Conf. on Advanced Technologies, Systems and Services in Telecomm. (TELSIKS)*, Nis, 2017, pp. 87-94.
8. H. Chou and J. W. Liu, "Synthesis and Characteristic Evaluation of Convex Metallic Reflectarray Antennas to Radiate Relatively Orthogonal Multibeams," *IEEE Trans. Antennas Propag.*, vol. 66, no. 8, pp. 4008-4016, Aug. 2018.
9. M. Jiang, Z. N. Chen, Y. Zhang, W. Hong, and X. Xuan, "Metamaterial-based thin planar lens antenna for spatial beamforming and multibeam massive MIMO," *IEEE Trans. Antennas Propag.*, vol. 65, no. 2, pp. 464–472, Feb. 2017.
10. E. G. Plaza, J. R. Costa, C. A. Fernandes, G. León, S. Loredo and F. Las-Heras, "A multibeam antenna for imaging based on planar lenses," *9th European Conference on Antennas and Propagation (EuCAP)*, Lisbon, 2015, pp. 1-5.
11. A. H. Abdelrahman, F. Yang, A. Z. Esherbeni, and P. Nayeri, *Analysis and Design of Transmitarray Antennas*, M&C Publishers, 2017.
12. M. Beccaria, A. Massaccesi, P. Pirinoli and Linh Ho Manh, "Multibeam transmitarrays for 5G antenna systems," *2018 IEEE Seventh International Conference on Communications and Electronics (ICCE)*, Hue, Vietnam, 2018, Jul 18-20, pp. 217-221.
13. M. Beccaria, A. Massaccesi, P. Pirinoli, N. K. Kiem, N. H. Trung and Linh Ho Manh, "Innovative MIMO Antennas for 5G Communication Systems," *2018 IEEE International Conference on Environment and Electrical Engineering and 2018 IEEE Industrial and Commercial Power Systems Europe (EEEIC / I&CPS Europe*, Palermo, Italy, 2018, June 12-15, pp. 1-4.
14. A. Massaccesi, P. Pirinoli, "Enhancing the bandwidth in transmitarray antennas using tapered transmission line matching approach". In *12th European Con-*

ference on Antennas and Propagation (EuCAP 2018), London, UK, 2018, Apr 9-13, pp. 1-4, IET.
15. A. Massaccesi, *et al.*, "3D-Printable dielectric transmitarray with enhanced bandwidth at millimeter-waves," *IEEE Access*, vol. 6, pp. 46407-46418, 2018.
16. A. Massaccesi, G. Dassano, and P. Pirinoli, "Beam Scanning Capabilities of a 3D-Printed Perforated Dielectric Transmitarray", Electronics, MDPI, vol. 8, no. 4, article no. 379, March 2019.